



# Randomness and changes of heart rate and respiratory frequency during high altitude mountain ascent without acclimatization

Eva Wesfreid<sup>a,b,\*</sup>, Véronique Billat<sup>c</sup>

<sup>a</sup> LMPA, Université du Littoral, Côte d'Opale, 62228 Calais, France

<sup>b</sup> CMLA, École Normale Supérieure de Cachan, 94235 Cachan, France

<sup>c</sup> Unité INSERM 902, Genopole-Université d'Évry Val d'Essonne, France

## ARTICLE INFO

### Article history:

Received 9 April 2011

Received in revised form 9 July 2011

Available online 8 September 2011

### Keywords:

Scaling behavior

Detrended fluctuation analysis

Local cosine 4 transform

Wavelet leaders

Heart rate

Respiratory frequency

## ABSTRACT

The aim of this study was to detect and compare the changes in the time–frequency and fractal scaling behaviors of heart rate (HR) and respiratory frequency (Rf), recorded simultaneously during a high altitude mountain ascent. The time–frequency analysis was performed using the local cosine4 orthonormal bases of Coifman, Malvar and Meyer, whose spectrum is not redundant as those computed with the short Fourier transform. The fractal scaling behavior was obtained using the detrended fluctuation (DFA) and the wavelet leaders (WL) analysis. Results showed that the high altitude mountain ascent differently affected HR and Rf variability. Rf average values increased ( $p = 0.0003$ ) while HR average values did not change. The scaling variability of HR was altered during the mountain ascent, which was detected by the increasing HR short range DFA exponents with altitude ( $p < 0.03$ ). Rf scaling variability remained unchanged. These differences between HR and Rf alterations were also observed for the local cosine4 power law behavior since power law exponents, in absolute values, increased for HR ( $p < 0.003$ ) while those of Rf did not change. Furthermore, the ratio of low over the whole local spectrum energy of Rf decreased with altitude ( $p = 0.04$ ) in contrast to HR. In most of these HR and Rf analyses, one of the two time series was significantly modified but not both. Moreover, the Rf local cosine4 spectrum had higher entropy compared to HR ( $p < 0.01$ ), the difference between the Rf and the HR entropy increased ( $p = 0.04$ ) during the mountain ascent. In consequence, Rf had more randomness than HR and altitude increased this difference.

© 2011 Elsevier B.V. All rights reserved.

## 1. Introduction

The detection of fatigue in mountain ascent could prevent accidents by encouraging Alpinists to stop for a recovery and/or immediately descend. Indeed, most accidents occur in the descent due to the Alpinist's exhaustion state. This becomes a major issue given that there are an ever increasing number of people who climb at an altitude of about 5000 m and these high-altitude ascents represent a major challenge for the majority of these subjects, as many are not acclimatized or accustomed to walking on icy and steep paths.

In Europe, one of the most popular summits is Mont Blanc (4808 m), with approximately 20,000 climbers each year. In general, the Mont Blanc ascent lasts 24 h, interspersed by a short rest night spent in a mountain hut at 3817 m. In a real condition experiment conducted during the Mont Blanc ascent with gas exchange measurements [1], we showed that the oxygen cost (i.e. the oxygen volume consumed for each meter) of walking increased substantially after 3000 m due to the combined effects of environmental conditions and fatigue. Furthermore, preliminary investigations performed on non elite

\* Corresponding author at: LMPA, Université du Littoral, Côte d'Opale, 62228 Calais, France.

E-mail address: [eva.theumann@gmail.com](mailto:eva.theumann@gmail.com) (E. Wesfreid).

**Table 1**

HR mean values with standard deviation for eight steps and ten Alpinists.

HR							
$E_1$	$E_2$	$E_3$	$E_4$	$E_5$	$E_6$	$E_7$	$E_8$
163.0 ± 35.6	134.5 ± 12.9	135.9 ± 8.8	145.4 ± 14.0	173.7 ± 22.3	166.6 ± 19.0	186.7 ± 14.3	179.9 ± 13.2
188.7 ± 15.0	198.9 ± 14.6	192.3 ± 10.8	192.0 ± 10.9	190.1 ± 19.4	180.9 ± 17.4	143.4 ± 13.2	149.9 ± 9.4
183.5 ± 22.1	179.9 ± 21.1	171.0 ± 14.3	172.1 ± 13.4	174.9 ± 19.6	176.9 ± 20.4	186.2 ± 20.6	170.0 ± 21.9
205.6 ± 12.4	185.5 ± 15.7	179.4 ± 10.8	180.8 ± 12.1	180.1 ± 19.7	174.9 ± 18.0		
167.06 ± 16.5	157.8 ± 10.9	173.0 ± 16.2	174.2 ± 16.7	166.5 ± 18.0	163.7 ± 17.3		
176.02 ± 13.2	175.9 ± 11.2	173.0 ± 20.3	191.1 ± 28.7	163.9 ± 9.5	157.3 ± 10.9		
207.00 ± 13.2	197.1 ± 14.3	176.0 ± 10.8	172.2 ± 11.4	170.3 ± 28.5	136.5 ± 15.6		
200.56 ± 10.7	196.3 ± 11.8	187.5 ± 11.6	179.3 ± 9.8	186.6 ± 10.9	184.6 ± 11.0		
200.08 ± 14.3	196.8 ± 14.8	199.4 ± 15.5	187.7 ± 19.4	197.2 ± 21.2	186.9 ± 21.7		
200.82 ± 12.2	195.7 ± 13.4	184.9 ± 13.0	187.8 ± 9.1	140.8 ± 5.6	144.6 ± 3.7		

**Table 2**

Rf mean values with standard deviation for eight steps and ten Alpinists.

Rf							
$E_1$	$E_2$	$E_3$	$E_4$	$E_5$	$E_6$	$E_7$	$E_8$
28.0 ± 9.1	39.7 ± 7.2	42.7 ± 7.9	48.1 ± 9.7	40.2 ± 9.9	44.9 ± 10.6	36.0 ± 7.4	42.3 ± 6.5
32.6 ± 7.4	41.1 ± 7.9	45.0 ± 7.7	51.4 ± 8.7	42.7 ± 10.2	47.9 ± 8.6	43.9 ± 8.3	46.0 ± 6.1
34.4 ± 8.9	34.6 ± 9.2	40.1 ± 9.8	42.0 ± 10.1	41.4 ± 9.9	40.4 ± 11.1	42.2 ± 11.6	47.1 ± 11.5
32 ± 8.8.4	39.3 ± 7.1	44.1 ± 7.0	44.5 ± 7.5	36.2 ± 8.6	38.3 ± 9.8		
29.3 ± 4.8	30.8 ± 5.2	30.7 ± 5.8	33.1 ± 7.2	35.4 ± 7.0	36.6 ± 7.8		
31.8 ± 4.7	35.0 ± 5.2	34.8 ± 8.0	30.3 ± 7.2	40.2 ± 7.5	40.0 ± 7.4		
27.5 ± 6.3	32.6 ± 6.7	33.2 ± 4.3	33.9 ± 3.9	30.5 ± 7.6	33.5 ± 6.6		
31.0 ± 5.4	33.9 ± 4.9	32.9 ± 5.2	33.1 ± 4.5	34.4 ± 5.9	37.1 ± 6.5		
27.7 ± 5.1	30.5 ± 5.6	29.1 ± 5.4	30.9 ± 5.1	34.1 ± 6.3	36.2 ± 5.4		
31.2 ± 3.9	34.0 ± 3.4	34.8 ± 4.3	36.7 ± 3.8	40.5 ± 3.7	43.5 ± 3.7		

runners completing the Paris marathon, showed a modification of the fractal behavior of the speed and heart rate power law scale relationship [2].

In exercise performed at altitude, the respiratory frequency becomes crucial for avoiding hypoxemia. Autonomic responses are also crucial for adaptation to hypoxia which triggers several autonomic mechanisms, mainly in the respiratory system [3]. Previous studies have evaluated heart autonomic response using heart rate variability (HRV) analysis in subjects exposed to acute hypobaric hypoxia in real conditions [4] as well as in simulated settings [5,6]. Acute exposure to high altitude induced alterations in heart and respiratory rates [3,4]. A prior study performed at 2700 and 3700 m above sea level for tourists who reached these altitudes by mechanical transport, showed that heart rate variability was altered [7–11]. Furthermore, we previously reported that the fractal behavior of the heart rate was altered at the end of a marathon which represents an endurance challenge in human races. However, the high altitude mountain ascent cumulates the effects of exercise duration with hypoxia. Furthermore, hypoxia induces a hyperventilation [1] meaning fractal behavior could be more affected by hypoxia than the heart rate. Therefore, the aim of this study was to detect and compare randomness and changes in the time–frequency and fractal scaling behaviors of heart rate and respiratory frequency during a high altitude mountain ascent for non acclimatized subjects.

## 2. Methods

### 2.1. Subjects

Ten healthy Alpinists participated in this study (Tables 1 and 2). They were familiar with high mountain walking, but this experiment was conducted at the beginning of the summer and still none of the subjects were acclimatized to altitude. Indeed, none of them had been exposed to altitude in the two months prior to the study. Before participation, all subjects were informed of the risks and stresses associated with the protocol, and gave their written voluntary informed consent. The present study conformed to the standards set by the *Declaration of Helsinki* and its procedures were approved by the local ethics committee of the Hospital Saint Louis of Paris.

### 2.2. Physiological measurements

The respiratory frequency and heart rate were simultaneously collected with the portable gas exchange analyzer K4b<sub>2</sub> [1]. The flow calibration was done at sea level and verified at the Gouter Hut (4000 m) before starting the final ascent to the summit on Sunday. The Cosmed K4b<sub>2</sub> allows the introduction of actual barometric pressure values and then to change air density, allowing appropriate usage in hypobaric conditions. The environmental and route conditions did not change during the study and the barometric pressure at sea-level remained at 765 mm Hg during the entire ascent. The breath-by-breath

data were smoothed using a 3-step average filter to enhance the underlying characteristics (Data management software, Cosmed, Rome, Italy) and then averaged every 30 s. The heart rate and breath rates were the inverse time interval between two successive breaths or beats.

### 2.3. Equipment

All subjects wore the same equipment and clothing (Millet, Annecy, France). Each subject carried a rucksack weighing 7 kg (males) and 5 kg (females) in addition to the gas exchange analyzer (800 gr K4b<sub>2</sub> Cosmed, Roma). The gas exchange analyzers were calibrated each morning before starting the ascent according to the manufacturer's instructions (K4b<sub>2</sub>, Cosmed, Roma) [12]. Breath-by-breath data were later reduced to 30 s averages. Data on heart rate and respiratory frequency were collected for each subject from the start of the Mont Blanc ascent (2372 m) at 11 am on Saturday, until arrival at the mountain hut (3817 m) at 5 pm on Saturday.

### 2.4. Protocol of climbing and data collection

Subjects were free to choose their own pace. Every two hours of climbing included a 25 and 15-min rest break. When the conditions turned to snow and ice (3200 m), subjects roped up and were again instructed to walk at their own pace. Both subjects and the guides were provided with instructions on how to place the mask of the K4b<sub>2</sub> and carried walkie-talkies to communicate with the experimental personnel.

Data collection continued on Sunday, commencing at 3 am and finishing at 8 am when the subjects attained the summit (4807 m). Individual baseline data were registered over a period of 5 min. Both altitude and vertical speed were measured using an altimeter, which also acts as a heart rate monitor (AXN700, Polar, Finland) and a GPS (Garmin, USA) receiver (12 satellites) into the K4b<sub>2</sub>. The Garmin GPS equipment computes vertical displacements from pressure changes detected with an incorporated altimeter. We verified that the two altimeters provided the same altitude. Vertical speed was calculated as the time spent to cover the 250 m separating the different steps. Heart rate and respiratory frequency were recorded simultaneously at each respiratory beat during an ascent of Mont Blanc in eight steep mountain steps ( $E_1, \dots, E_8$ ) starting from 2500 m of altitude to 4500 m over steps of 250 m of altitude ( $E_1 = 2500\text{--}2750$  m;  $E_2 = 2751\text{--}3000$  m;  $E_3 = 3001\text{--}3250$  m;  $E_4 = 3251\text{--}3500$  m;  $E_5 = 3501\text{--}3750$  m;  $E_6 = 3751\text{--}4000$  m;  $E_7 = 4001\text{--}4250$  m;  $E_8 = 4251\text{--}4500$  m).

We computed the ratio between respiratory frequency (resp. heart rate) and vertical speed that gave the number of breaths (breath. m<sup>-1</sup>) and cardiac beats (beat. m<sup>-1</sup>) required for climbing one meter.

### 2.5. Statistics

The HR and Rf variability parameters obtained at each stage of altitude were analyzed using ANOVA, analysis of variance, followed by a post hoc Bonferroni test to establish differences between groups over mountain steps. Statistical significance was set at  $p \leq 0.05$ .

## 3. Mathematics analysis

Heart rate (HR) and respiratory frequency (Rf) are non stationary time series, their time frequency behavior can be obtained using a local, Fourier or trigonometric transform. We choose the local cosine<sub>4</sub> orthonormal basis, constructed by Coifman, Malvar and Meyer [8–11], to analyze the HR and Rf time series over a time segmentation into boxes of 128 samples. The spectrum obtained using this orthonormal basis is not redundant as the one computed with the short Fourier transform. The signal energy is thus split into the sum of the local cosine<sub>4</sub> spectrum energies. This signal analysis was used to estimate power law exponents, entropy and low over whole energy values of the local cosine<sub>4</sub> spectrum over the time segmentation boxes.

The detrended fluctuation analysis (DFA) introduced by Peng et al. [13,14] estimates the root-mean square detrended fluctuations of the integrated time series over a time segmentation into boxes of equal length,  $n$ , with  $n_1 \leq n \leq n_2$ . This algorithm was performed in this study to estimate the HR and Rf timescale power law exponents of Alpinists in a Mont Blanc ascent. Moreover, the wavelet leaders proposed by Jaffard [15] to improve multifractal analysis [16,17], were used in this paper to estimate the HR and Rf power law scaling exponents.

### 3.1. Local cosine<sub>4</sub> transform

We describe briefly the local cosine<sub>4</sub> transform over the segmented time axis  $Z = \bigcup_{j \in Z} I_j$  into boxes  $I_j = [a_j, a_{j+1}[$  of length  $l_j = a_{j+1} - a_j$ .

As in Ref. [4], let us define the following rising cutoff function

$$r(t) = \begin{cases} 0 & \text{if } t \leq -1 \\ \sin \left[ \frac{\pi}{4} \left( 1 + \sin \frac{\pi}{2} t \right) \right] & \text{if } -1 < t < 1 \\ 1 & \text{if } t \geq 1 \end{cases}$$

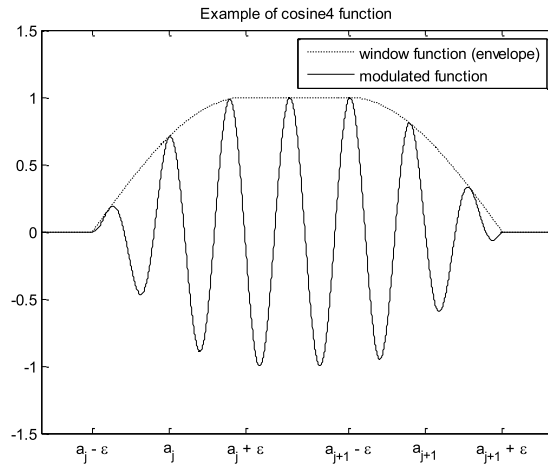


Fig. 1. Local cosine4 function over  $I_j = [a_j, a_{j+1}]$ .

which rises from being identically zero to being identically one and the window function  $w_j(t) = r(\frac{t-a_j}{\epsilon})r(\frac{a_{j+1}-t}{\epsilon})$  supported on the time interval  $[a_j - \epsilon, a_{j+1} + \epsilon]$  with  $\epsilon < \frac{l_j}{2}$ .

By modulating the window functions  $w_j(t)$ , we obtain the following local cosine4 functions

$$\Psi_k^j(n) = w_j\left(n + \frac{1}{2}\right) \sqrt{\frac{2}{l_j}} \cos \frac{\pi}{l_j} \left(k + \frac{1}{2}\right) \left[\left(n + \frac{1}{2}\right) - a_j\right]$$

which generate  $l^2(Z)$ , the set of functions  $f$  defined over  $Z$  with finite energy  $\sum_{n \in Z} |f(n)|^2 < \infty$ . Fig. 1 shows a cosine4 function.

The set of functions,  $\Psi_k^j$ , with  $j \in Z$  and  $k \in N$  is an orthonormal basis of  $l^2(Z)$ , consequently each time series  $f \in l^2(Z)$  can be decomposed into this basis,

$$f(n) = \sum_{j \in Z} \sum_{k \in N} c_{j,k} \Psi_k^j(n)$$

with

$$c_{j,k} = \langle f, \Psi_k^j \rangle = \sum_{j \in Z} \sum_{k \in N} f(n) \Psi_k^j(n)$$

where  $j \in Z$  denotes the time box and  $k \in N$  the frequency variable. The set of coefficients  $c_{j,k}$  with  $j \in Z$  and  $k \in N$  is the local cosine4 spectrum of  $f$ . Therefore  $f \rightarrow c_{j,k} \rightarrow f$  is the local cosine4 transform and its inverse.

### 3.2. Local cosine4 power law exponents

In this study, we used time segmentations into boxes of the same length  $L$ .

A finite time series  $s = s(n)_{1 \leq n \leq N}$  of length  $N$  is truncated to  $s(n)_{1 \leq n \leq N_1}$  where  $N_1 = \lfloor \frac{N}{L} \rfloor * L$ .

The local cosine4 spectrum of  $s$  verify a local power law if

$$|c_{j,k}| \approx \gamma_j k^{\beta_j}$$

or, equivalently

$$\log_2 |c_{j,k}| \approx \beta_j \log_2(k) + \log_2(\gamma_j)$$

where  $\gamma_j$  is a constant on each time-box,  $j$  denotes the time-box index ( $1 \leq j \leq n_b$ ), and  $k$  the frequency variable ( $1 \leq k \leq L$ ).

In this search, the HR and Rf time series of length  $N$ , recorded in the mountain ascent, were analyzed using this local cosine4 transform over a segmented time support into  $n_b$  boxes of length  $L = 128$ . For each HR and Rf time series the local power law exponents  $\beta_j$  were estimated as the slope of the line segment

$$y_j = \beta_j \log_2(k) + \log_2(\gamma_j)$$

that fits  $\log_2 |c_{j,k}|$  vs.  $\log_2(k)$  in a least-square sense for  $1 \leq k \leq L$ .

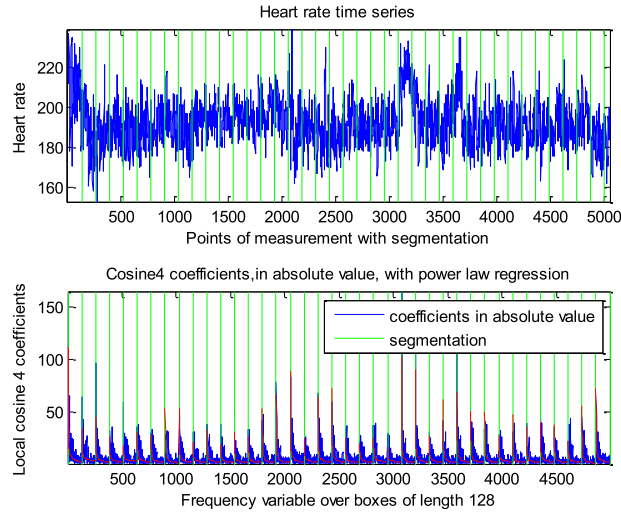


**Fig. 2.** Local cosine4 coefficients with power law regression.

Fig. 2 shows at the top a heart rate time series, and at the bottom the local cosine4 coefficients,  $(c_{j,k})_{1 \leq k \leq L}$  in absolute values, over the segmented time-support into  $n_b$  boxes,  $I_j = [a_j, a_{j+1}[$  with  $1 \leq j \leq n_b$ . Its power law regression curve,  $z = 2^j$  was superposed.

For each time series  $s$  (HR or Rf), we denote:  $\beta_j^s$ , its local power law exponent over the time segmentation box  $I_j$  and  $c_j^s = (c_{j,k}^s)_{1 \leq k \leq L}$ , its local cosine4 spectrum,

$$e_j^s = \sum_{k=1}^L |c_{j,k}^s|^2, \quad \text{its local spectrum energy over } I_j,$$

$$a_j^s = \frac{\sum_{k=1}^{L/2} |c_{j,k}^s|^2}{e_j^s}, \quad \text{its ratio of low over whole local spectrum energy over } I_j,$$

$$b_j^s = \frac{\sum_{k=L/2+1}^L |c_{j,k}^s|^2}{e_j^s}, \quad \text{its ratio of high over whole local spectrum energy over } I_j,$$

$$(a_j^{HR} + b_j^{HR} = 1 \text{ and } a_j^{Rf} + b_j^{Rf} = 1).$$

We can check that  $\|f\|^2 = \sum_{k=1}^L \|e_j^s\|^2$ , i.e. the signal energy  $\|f\|^2$  is decomposed into the sum of the local spectrum energies  $\|e_j^s\|$ .

### 3.2.1. Local spectrum entropy

The local spectrum entropy [2,4] over a segmentation box  $I_j$ :

$$d_j^s = - \sum_{k=1}^L \frac{|c_{j,k}^s|^2}{e_j^s} \log \left( \frac{|c_{j,k}^s|^2}{e_j^s} \right)$$

measures the rate of decay of the coefficients in absolute values, rearranged into decreasing order. Its value should be large when the coefficients are *mostly uniformly* distributed and small otherwise.

### 3.3. DFA (detrended fluctuation analysis)

DFA computes the root-mean square detrended fluctuations values of the integrated time series over a time segmentation onto boxes of length  $n$  ( $n$  is the time scale).

Each time series  $f$  of length  $N$  and mean value  $f_0$  is first integrated,

$$y[k] = \sum_{j=1}^{j=k} (f(j) - f_0).$$

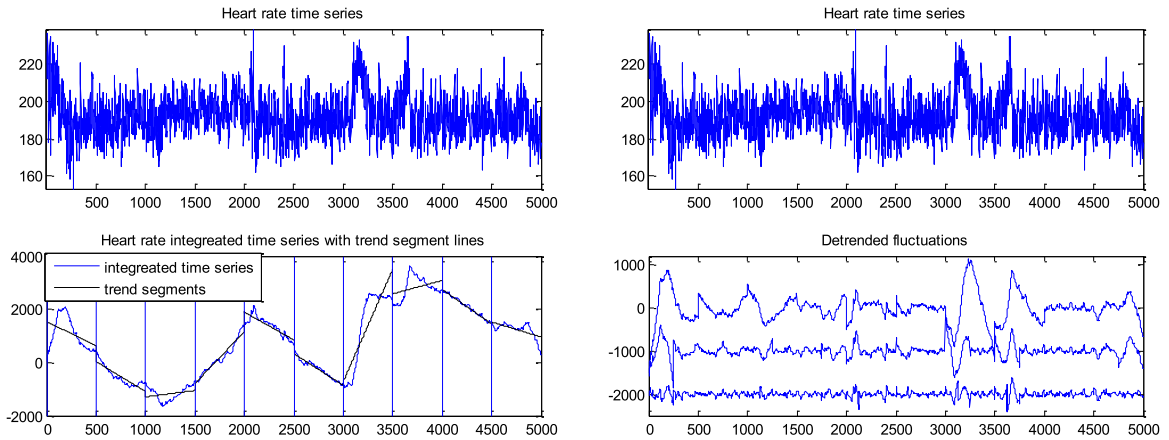


Fig. 3. Local linear trends and detrended fluctuations.

Its time support  $[1, N]$  is segmented into  $M$  non overlapping time boxes,  $I_j = [a_j, a_{j+1}[$ , of equal length  $n = a_{j+1} - a_j$  such that

$$\bigcup_{j=1}^M I_j = [1, nM]$$

with  $nM$  the largest multiple of  $n$  less than or equal to  $N$ .

The integrated time series  $y = y(k)_{1 \leq k \leq nM}$  is first approached by a piecewise linear time series  $y_n(k)_{1 \leq k \leq nM}$  such that its restriction to each time box  $I_j$  is a line segment that fits  $y(k)_{k \in I_j}$  in a least square sense, and then detrended  $g = y - y_n$ :

$$g = (g(k))_{1 \leq k \leq nM} = (y(k) - y_n(k))_{1 \leq k \leq nM}$$

across a range of timescales,  $n_1 \leq n \leq n_2$ .

Fig. 3 shows a heart rate time series recorded on the Mont Blanc ascent between 3001 and 3500 m of altitude, at the top is the integrated time series with trend segments over boxes of length  $n = 500$ , on the bottom (left) and three detrended fluctuation time series obtained with boxes of length (time scales)  $n = 500, 250$  and  $125$  on the bottom (right). The root-mean square detrended fluctuations of the integrated time series over timescales  $n$ :

$$F[n] = \sqrt{\frac{1}{m} \sum_{k=1}^m |y(k) - y_n(k)|^2} \tag{1}$$

verify a scaling power law if

$$F[n] \approx cn^\alpha$$

or, equivalently

$$\log(F[n]) \approx \alpha \log(n) + \log(c)$$

for a range of timescales  $n_1 \leq n \leq n_2$ .

The timescaling exponent  $\alpha$  can therefore be estimated as the slope of the line segment

$$z = \alpha \log(n) + \log(c)$$

over the range of scales  $[n_1, n_2]$ .

In this HR and Rf analysis, two timescaling exponents were estimated, a short range,  $\alpha_1$  for  $n \in [4, 11[$  and a long range,  $\alpha_2$  for  $n \in [11, 181[$ , Fig. 4 shows these two exponents.

### 3.4. Wavelet leaders scaling exponents [15–17]

Wavelet leaders are based on discrete wavelet coefficients [8] using an orthogonal wavelet function  $\Psi(t)$  with compact support and  $n$  vanishing moments:

$$\int_{-\infty}^{+\infty} t^k \Psi(t) dt = 0 \quad \text{for } k \in \{1, 2, \dots, n-1\} \quad \text{and} \quad \int_{-\infty}^{+\infty} t^n \Psi(t) dt \neq 0$$

(we choose the Daubechies wavelet with  $n = 5$  vanishing moments).

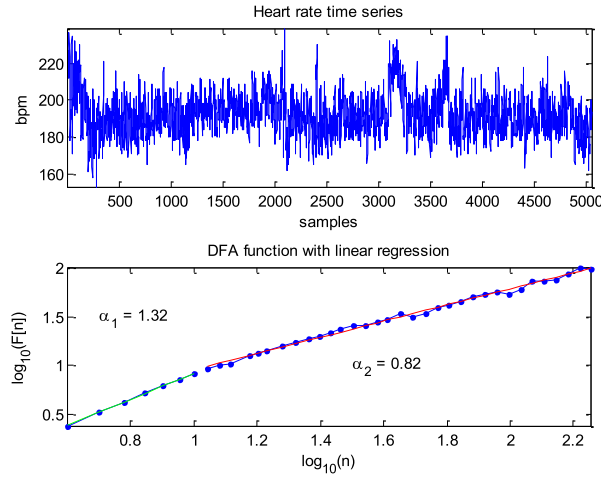


Fig. 4. DFA function with short and long range exponents.

The set of normalized wavelets, translated to position  $2^j k$  and dilated to scale  $s = 2^j$ :

$$\left\{ \Psi_{j,k}(t) = \frac{1}{2^j} \Psi \left( \frac{t}{2^j} - k \right), j \in Z, k \in Z \right\}$$

is an orthogonal basis of  $L^2(R)$ . Thus any function  $f \in L^2(R)$  can be decomposed in this basis:

$$f(t) = \sum_{j,k} c_{j,k} \Psi \left( \frac{t}{2^j} - k \right)$$

with

$$c_{j,k} = \frac{1}{2^j} \int_{-\infty}^{+\infty} f(t) \Psi \left( \frac{t}{2^j} - k \right).$$

The wavelet leaders,  $L_f(j, k)$  for each scale  $2^j$  and position  $2^j k$  were computed as the maximum of the discrete wavelet coefficients in absolute values,  $|c_{j,k}|$ , in a time neighborhood

$$3\lambda = \lambda_{j,k-1} \cup \lambda_{j,k} \cup \lambda_{j,k+1}$$

of  $\lambda = \lambda_{j,k} = [2^j k, 2^j(k+1)[$  overall finer scales  $2^i < 2^j$  ( $f$  denotes the time series  $j \in Z, k \in Z$ ):

$$L_\lambda = L_f(j, k) = \sup_{\mu \subset 3\lambda} |c_\mu|. \tag{2}$$

For example,  $L_f(3, 3)$  is the maximum value of the set of coefficients in the gray area:

The wavelet leaders increase with the scales  $2^j$  which improves significantly the power law scaling behavior of the structure function

$$S_f(j, q) = \frac{1}{n_j} \sum_{k=1}^{n_j} L_f(j, k)^q \approx c_q (2^j)^{\tau(q)} \tag{3}$$

or, equivalently:

$$\log_2(S_f(j, q)) \approx \tau(q)j + \log_2(c_q) \tag{4}$$

where  $n_j \approx N/2^j$  is the number of such coefficients for a range of scales  $s = 2^j$  with  $j \in [j_1, j_2]$ .

Fig. 10 compares the structure functions,  $S_f(j, q)$ , of a heart rate time series in a log–log plot using wavelet coefficients (on the left) and wavelet leaders (on the right).

#### 4. Results

Overall results showed that HR and Rf time series were differently affected during a high altitude mountain ascent.

We analyzed HR and Rf time series of ten Alpinists, simultaneously recorded during a Mont Blanc ascent, from 2500 to 4500 m of altitude. Seven time series were badly recorded between 4000 and 4500 m altitude. Therefore, the time and time–frequency analysis was done over 6 steps,  $E_1, E_2, E_3, \dots, E_6$ , (resp. 8 steps,  $E_1, E_2, E_3, \dots, E_8$ ) of 250 m of altitude from

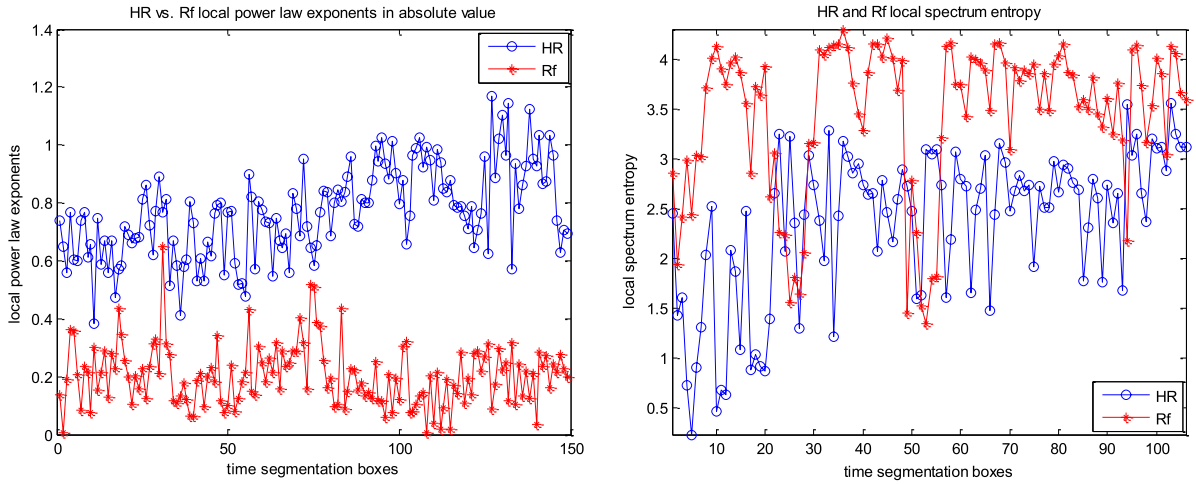


Fig. 5. HR vs. Rf local power law exponents and local entropy.

2500 to 4000 m (resp. from 2500 to 4500 m) for 7 Alpinists (resp. 3 Alpinists). Otherwise, the DFA and WL scaling analysis needs a longer time series, thus this analysis was done over 3 steps (resp. 4 steps) of 500 m of altitude from 2500 to 4000 m (resp. from 2500 to 4500 m) for 7 Alpinists (resp. 3 Alpinists).

The average HR time series were not modified by altitude in contrast to Rf whose average values increased significantly ( $p = 0.0003$ ). Table 1 (resp. Table 2) shows the HR (resp. Rf) mean and standard deviation (SD) values for the ten Alpinists (one row per Alpinist).

#### 4.1. Cosine4 transform results

##### 4.1.1. Local power law exponent behavior

The HR and Rf local spectrum has no characteristic frequencies as speech or music time series. Therefore, the local cosine4 coefficients, in absolute values,  $|c_{j,k}|$ , were approached by scaling power law curves:

$$|c_{j,k}| \approx \gamma_j k^{\beta_j}$$

where  $1 \leq k \leq L$  for each  $n_b$  time segmentation box  $I_j$  ( $1 \leq j \leq n_b$ ).

The power law exponents,  $\beta_j$ , were estimated as the slope of the line segments

$$y = \beta_j \log(k) + \log(\gamma_j).$$

We observed that each HR and Rf power law curve decreased:

$$\beta_j^{HR} < 0 \text{ and } \beta_j^{Rf} < 0 \text{ for all time boxes } I_j \text{ and}$$

$$|\beta_j^{HR}| > |\beta_j^{Rf}| \text{ and } |\beta_j^{HR}| - |\beta_j^{Rf}| \text{ increases } (p = 0.05) \text{ with altitude.}$$

The Rf local spectrum is therefore more uniformly distributed compared with HR and this difference increases during the mountain ascent. Moreover,  $|\beta_j^{HR}|$  increases significantly with altitude ( $p < 0.003$ ) but not  $|\beta_j^{Rf}|$ . This is shown in Fig. 5 on the left, for one Alpinist.

Table 3 (resp. Table 4) shows the mean and SD values of the power law exponents  $\beta_j^{HR}$  (resp.  $\beta_j^{Rf}$ ) for the ten Alpinists (one row per Alpinist).

##### 4.1.2. Ratio of low over whole local spectrum energy

This ratio of low ( $1 \leq k \leq L/2$ ) over whole ( $1 \leq k \leq L$ ) local frequency energy (defined in 3.2) was computed for each HR and Rf time series over the  $n_b$  time segmentation boxes  $I_j$ . We observed that for each  $j$  ( $1 \leq j \leq n_b$ ),  $a_j^{HR} > a_j^{Rf}$ ,  $0.88 < a_j^{HR} < 0.99$ , and  $0.65 < a_j^{Rf} < 0.81$ . The values of  $a_j^{HR}$  are closer to 1 compared with  $a_j^{Rf}$  and

$$\sum_{k=1}^{L/2} |c_{j,k}^{HR}| = p e_j^{HR} \quad 0.88 < p < 0.99$$

$$\sum_{k=1}^{L/2} |c_{j,k}^{Rf}| = p e_j^{Rf} \quad 0.65 < p < 0.81$$

( $e_j^s = \sum_{k=1}^L |c_{j,k}^s|^2$  (resp.  $\sum_{k=1}^{L/2} |c_{j,k}^s|^2$ ) is the local spectrum (resp. the low frequency) energy of a signal  $s$  over  $I_j$ ).

**Table 3**  
 $\beta_j^{HR}$  mean values with standard deviation for eight steps and ten Alpinists.

HR							
$E_1$	$E_2$	$E_3$	$E_4$	$E_5$	$E_6$	$E_7$	$E_8$
$-0.77 \pm 0.13$	$-0.85 \pm 0.12$	$-0.92 \pm 0.13$	$-0.93 \pm 0.08$	$-0.83 \pm 0.11$	$-0.79 \pm 0.15$	$-0.68 \pm 0.12$	$-0.78 \pm 0.12$
$-0.64 \pm 0.11$	$-0.70 \pm 0.11$	$-0.63 \pm 0.11$	$-0.67 \pm 0.12$	$-0.82 \pm 0.11$	$-0.84 \pm 0.11$	$-0.92 \pm 0.21$	$-0.90 \pm 0.15$
$-0.76 \pm 0.12$	$-0.76 \pm 0.10$	$-0.72 \pm 0.11$	$-0.73 \pm 0.09$	$-0.73 \pm 0.13$	$-0.76 \pm 0.11$	$-0.76 \pm 0.08$	$-0.82 \pm 0.13$
$-0.71 \pm 0.09$	$-0.74 \pm 0.16$	$-0.62 \pm 0.11$	$-0.67 \pm 0.12$	$-0.80 \pm 0.10$	$-0.7 \pm 0.11$		
$-0.33 \pm 0.05$	$-0.44 \pm 0.10$	$-0.62 \pm 0.10$	$-0.72 \pm 0.15$	$-0.77 \pm 0.14$	$-0.71 \pm 0.14$		
$-0.70 \pm 0.11$	$-0.59 \pm 0.12$	$-0.81 \pm 0.03$	$-0.83 \pm 0.15$	$-0.68 \pm 0.12$	$-0.70 \pm 0.07$		
$-0.64 \pm 0.12$	$-0.78 \pm 0.11$	$-0.63 \pm 0.10$	$-0.68 \pm 0.12$	$-0.73 \pm 0.14$	$-0.91 \pm 0.17$		
$-0.64 \pm 0.12$	$-0.58 \pm 0.06$	$-0.69 \pm 0.04$	$-0.46 \pm 0.21$	$-0.52 \pm 0.15$	$-0.58 \pm 0.10$		
$-0.48 \pm 0.12$	$-0.61 \pm 0.07$	$-0.48 \pm 0.11$	$-0.63 \pm 0.06$	$-0.70 \pm 0.07$	$-0.71 \pm 0.11$		
$-0.65 \pm 0.06$	$-0.73 \pm 0.07$	$-0.69 \pm 0.12$	$-0.59 \pm 0.12$	$-0.80 \pm 0.13$	$-0.79 \pm 0.11$		

**Table 4**  
 $\beta_j^{Rf}$  mean values with standard deviation for eight steps and ten Alpinists.

Rf							
$E_1$	$E_2$	$E_3$	$E_4$	$E_5$	$E_6$	$E_7$	$E_8$
$-0.19 \pm 0.13$	$-0.21 \pm 0.06$	$-0.19 \pm 0.09$	$-0.18 \pm 0.09$	$-0.25 \pm 0.11$	$-0.28 \pm 0.09$	$-0.25 \pm 0.07$	$-0.18 \pm 0.11$
$-0.21 \pm 0.11$	$-0.24 \pm 0.09$	$-0.16 \pm 0.08$	$-0.21 \pm 0.11$	$-0.22 \pm 0.13$	$-0.15 \pm 0.09$	$-0.21 \pm 0.09$	$-0.21 \pm 0.07$
$-0.19 \pm 0.11$	$-0.26 \pm 0.09$	$-0.18 \pm 0.10$	$-0.16 \pm 0.10$	$-0.23 \pm 0.15$	$-0.21 \pm 0.11$	$-0.27 \pm 0.12$	$-0.23 \pm 0.12$
$-0.15 \pm 0.16$	$-0.26 \pm 0.12$	$-0.18 \pm 0.13$	$-0.13 \pm 0.09$	$-0.13 \pm 0.15$	$-0.00.09$		
$-0.29 \pm 0.07$	$-0.24 \pm 0.14$	$-0.22 \pm 0.10$	$-0.16 \pm 0.15$	$-0.20 \pm 0.12$	$-0.16 \pm 0.06$		
$-0.34 \pm 0.10$	$-0.26 \pm 0.09$	$-0.27 \pm 0.08$	$-0.24 \pm 0.17$	$-0.22 \pm 0.17$	$-0.18 \pm 0.15$		
$-0.25 \pm 0.12$	$-0.30 \pm 0.13$	$-0.26 \pm 0.11$	$-0.34 \pm 0.16$	$-0.29 \pm 0.14$	$-0.27 \pm 0.11$		
$-0.27 \pm 0.08$	$-0.12 \pm 0.08$	$-0.17 \pm 0.06$	$-0.19 \pm 0.13$	$-0.21 \pm 0.11$	$-0.21 \pm 0.15$		
$-0.17 \pm 0.18$	$-0.28 \pm 0.14$	$-0.27 \pm 0.13$	$-0.33 \pm 0.10$	$-0.24 \pm 0.16$	$-0.08 \pm 0.15$		
$-0.15 \pm 0.13$	$-0.17 \pm 0.10$	$-0.16 \pm 0.15$	$-0.15 \pm 0.09$	$-0.25 \pm 0.10$	$-0.19 \pm 0.10$		

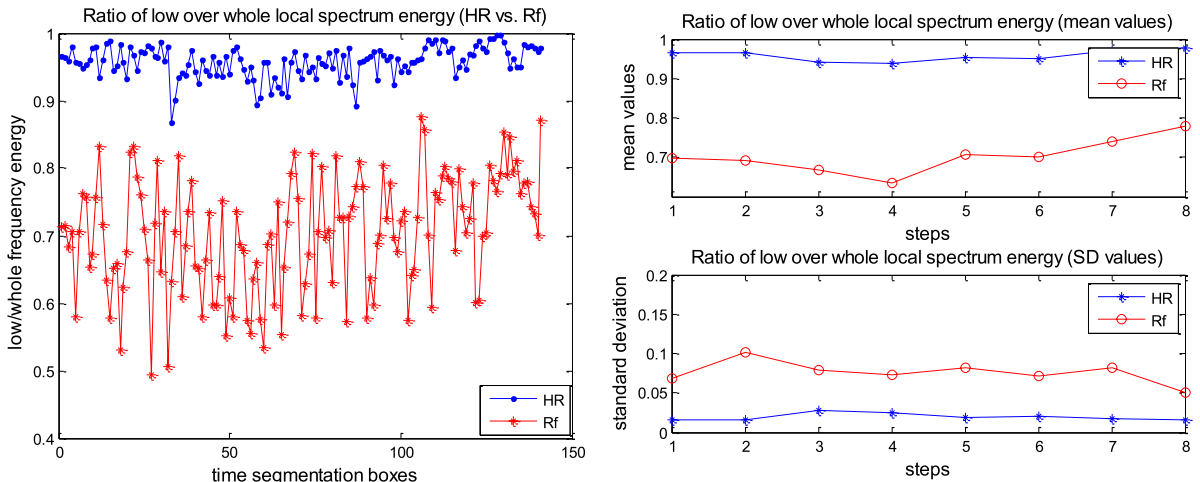


**Fig. 6.** Low frequency energy.

Moreover,  $SD(a^{Rf}) > SD(a^{HR})$ .

We show  $a^{HR} = (a_j^{HR})_{1 \leq j \leq n_b}$  and  $a^{Rf} = (a_j^{Rf})_{1 \leq j \leq n_b}$  in Fig. 6 on the left, its mean and standard deviation (SD) values on the right. This analysis shows that the Rf ratio,  $a_j^{Rf}$ , has a rough behavior compared with the HR one. Table 5 (resp. Table 6) shows  $mean(a^{HR})/mean(a^{Rf})$  (resp.  $std(a^{HR})/std(a^{Rf})$ ) for the ten Alpinists (one row per Alpinist) to be compared.

4.1.3. Local spectrum entropy

The local spectrum entropy,  $d^s = (d_j^s)_{1 \leq j \leq n_b}$  over the time segmentation boxes, with

$$d_j^s = - \sum_{k=1}^L \frac{|c_{j,k}^s|^2}{e_j^s} \log \left( \frac{|c_{j,k}^s|^2}{e_j^s} \right)$$

**Table 5**mean( $a_j^{HR}$ )/mean( $a_j^{Rf}$ ) values for eight steps and ten Alpinists.

$E_1$	$E_2$	$E_3$	$E_4$	$E_5$	$E_6$	$E_7$	$E_8$
0.9/0.70	0.98/0.74	0.97/0.69	0.98/0.64	0.97/0.75	0.96/0.73	0.95/0.72	0.95/0.67
0.95/0.77	0.94/0.81	0.93/0.69	0.93/0.72	0.97/0.74	0.97/0.63	0.99/0.67	0.97/0.71
0.96/0.70	0.97/0.69	0.94/0.67	0.94/0.63	0.95/0.71	0.95/0.70	0.97/0.74	0.98/0.78
0.95/0.68	0.97/0.74	0.92/0.66	0.93/0.57	0.96/0.65	0.96/0.55		
0.87/0.71	0.80/0.66	0.92/0.64	0.93/0.61	0.95/0.67	0.95/0.60		
0.94/0.76	0.92/0.70	0.97/0.78	0.98/0.70	0.93/0.64	0.93/0.64		
0.92/0.70	0.95/0.77	0.92/0.74	0.93/0.74	0.98/0.74	0.99/0.72		
0.92/0.69	0.93/0.64	0.94/0.70	0.92/0.68	0.90/0.77	0.93/0.67		
0.86/0.64	0.90/0.71	0.87/0.72	0.91/0.73	0.97/0.70	0.97/0.60		
0.93/0.70	0.94/0.70	0.95/0.66	0.93/0.65	0.96/0.69	0.97/0.65		

**Table 6**SD( $a_j^{HR}$ )/SD( $a_j^{Rf}$ ) values for eight steps and ten Alpinists.

$E_1$	$E_2$	$E_3$	$E_4$	$E_5$	$E_6$	$E_7$	$E_8$
0.01/0.12	0.02/0.10	0.02/0.12	0.01/0.09	0.01/0.12	0.02/0.05	0.01/0.08	0.02/0.09
0.02/0.08	0.03/0.10	0.02/0.13	0.03/0.12	0.01/0.14	0.01/0.08	0.02/0.11	0.03/0.04
0.02/0.07	0.02/0.10	0.03/0.08	0.02/0.07	0.02/0.08	0.02/0.07	0.02/0.08	0.02/0.05
0.03/0.12	0.01/0.10	0.03/0.10	0.02/0.06	0.02/0.13	0.01/0.07		
0.06/0.04	0.08/0.07	0.04/0.07	0.04/0.12	0.02/0.10	0.03/0.08		
0.02/0.14	0.03/0.07	0.01/0.07	0.00/0.13	0.02/0.11	0.01/0.06		
0.03/0.09	0.03/0.12	0.02/0.07	0.02/0.09	0.02/0.11	0.00/0.07		
0.02/0.06	0.01/0.09	0.02/0.05	0.02/0.05	0.03/0.10	0.02/0.07		
0.04/0.12	0.03/0.10	0.03/0.12	0.02/0.06	0.01/0.13	0.00/0.10		
0.01/0.08	0.02/0.09	0.01/0.13	0.02/0.09	0.03/0.09	0.01/0.09		

**Table 7**

HR local spectrum entropy/Rf local spectrum entropy.

$E_1$	$E_2$	$E_3$	$E_4$	$E_5$	$E_6$	$E_7$	$E_8$
1.31/3.25	1.85/3.01	2.46/3.55	2.62/3.88	2.51/2.73	2.53/3.75	3.02/3.48	3.17/3.77
2.63/2.93	2.99/2.53	3.15/3.26	3.10/3.29	2.71/2.49	2.87/3.88	1.04/3.67	1.74/3.49
2.43/3.78	2.18/3.65	3.05/3.92	3.15/4.04	2.84/3.74	2.90/3.95	1.93/3.74	1.94/3.66
2.50/3.66	2.08/3.27	3.19/3.79	3.25/4.04	2.74/3.15	2.85/4.06		
3.02/3.86	3.47/3.91	3.42/3.98	3.15/3.85	3.04/3.56	2.95/4.00		
3.34/3.27	3.46/3.71	2.14/3.22	2.17/3.59	3.18/3.87	3.21/4.05		
3.34/3.27	3.46/3.71	2.14/3.22	2.17/3.59	3.18/3.87	3.21/4.05		
3.52/3.87	3.41/4.00	3.26/3.87	3.59/3.95	3.57/3.13	3.41/3.88		
3.55/3.80	3.17/3.55	3.44/3.31	3.34/3.76	2.10/3.72	2.05/3.87		
3.43/3.76	3.15/3.67	3.17/3.69	3.42/3.86	2.17/3.52	2.07/3.71		

measures the local spectrum distribution inside each time segmentation box  $I_j$ , its value should be large when the coefficients are mostly uniformly distributed and smaller otherwise. The Rf local cosine4 spectrum had a higher local spectrum entropy compared to HR ( $p < 0.01$ ), thus was more uniformly distributed (as was found using the local power law exponents). The Rf time series seem to be more random than HR.

Fig. 5 shows on the right, a HR vs. Rf local spectrum entropy behavior for one Alpinist. Table 7 shows the HR vs. Rf local spectrum entropy values for the ten Alpinists (one row per Alpinist).

Heart rate is less random than respiratory frequency and altitude increased this difference. Fig. 7 shows the difference between the Rf and the HR spectrum entropies,  $D = d^{Rf} - d^{HR}$ , for two different Alpinists, this difference increases significantly ( $p = 0.04$ ) with altitude.

#### 4.2. Scaling behavior via DFA

The DFA functions  $F[n]$ , were computed for each HR and Rf time series. We observed that the DFA functions were smaller for the Rf compared with HR,  $F^{Rf}[n] < F^{HR}[n]$ , for most of the time scale values  $n$  and for most Alpinists. This behavior is shown in Fig. 8 for one alpinist over three steps.

For each HR and each Rf time series, two timescaling exponents were estimated, the short range  $\alpha_1^s$ , for  $n \in [4, 11[$  and the long range  $\alpha_2^s$ , for  $n \in [11, 181[$  with  $s = HR$  or  $s = Rf$ .

The estimated HR short range scaling exponents,  $\alpha_1^{HR}$ , were between 0.95 and 1.62, mostly greater than 1, while the estimated Rf short range scaling exponents,  $\alpha_1^{Rf}$ , were between 0.55 and 0.84. The HR short range exponents increased after an altitude of 3000 m ( $p < 0.03$ ), so the variability of HR was altered during the mountain ascent in contrast to Rf.

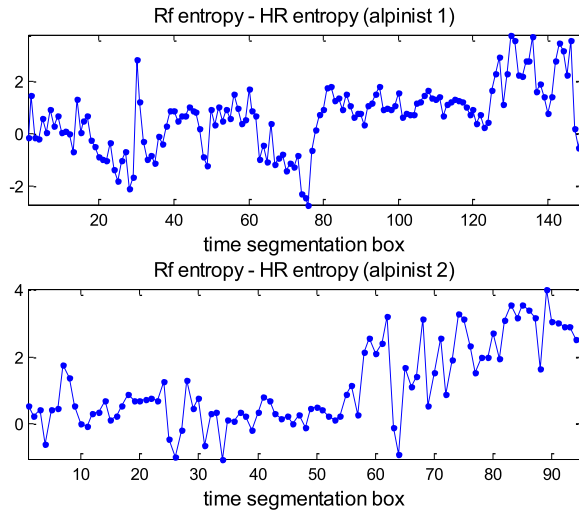


Fig. 7. Entropy (Rf)–entropy (HR) over time segmentation boxes.

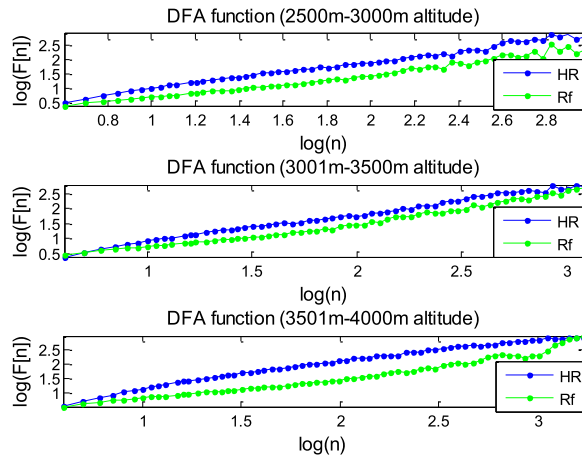


Fig. 8. HR vs. Rf DFA function.

Moreover,

$$\alpha_1^{HR} \geq \alpha_2^{HR} \text{ for each Alpinist and each step,}$$

$$\alpha_1^{Rf} \leq \alpha_2^{Rf} \text{ for 8 out of 10 Alpinists in } E_1, \text{ 9 out of 10 Alpinists in } E_2 \text{ and all Alpinists in } E_3.$$

$$\alpha_1^{HR} > \alpha_1^{Rf} \text{ for each Alpinist and each step.}$$

Fig. 9 shows the HR (on the left) and Rf (on the right) short and long range scaling exponents over three steps (9th line, Tables 8 and 9).

Table 8 (resp. Table 9) shows the HR vs. Rf short (resp. long) DFA scaling exponents:  $\alpha_1^{HR}(j)/\alpha_1^{Rf}(j)$  (resp.  $\alpha_2^{HR}(j)/\alpha_2^{Rf}(j)$ ) for ten Alpinists (one row per alpinist) over three or four steps.

### 4.3. Scaling behavior via wavelet leaders

The wavelet transform takes its maximum values near sharp signal variations. The wavelet leaders (2) increase with the scales  $s = 2^j$  which improves significantly the power law scaling behavior of its structure function (3) compared with the wavelet structure function. Fig. 10 shows both structure functions in a (log–log) representation (4) for HR and Rf time series over three steps with  $q = 2$ .

For each Alpinist, we estimated the short range scaling exponent  $\tau_1^s$ , for  $j \in [1, 3]$  and the long range scaling exponent  $\tau_2^s$ , for  $j \in [4, 7]$  over three or four steps of 500 m from 2500 to 4000 m or 4500 m of altitude with  $s = HR$  or  $s = Rf$ . Like DFA scaling exponents we find:

$$\tau_1^{HR} > \tau_1^{Rf} \text{ for each Alpinist and each step}$$

$$\tau_1^{HR} > \tau_2^{HR} \text{ for each alpinist and each step,}$$

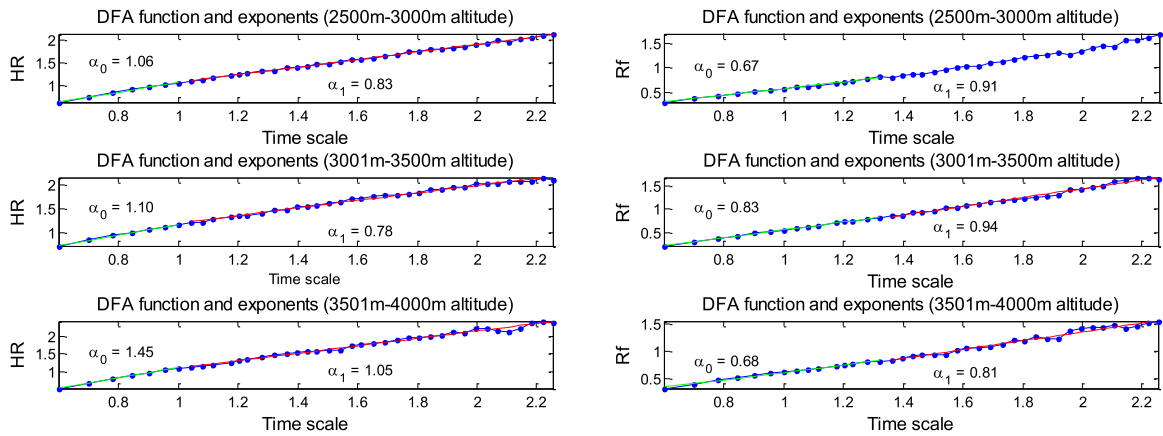


Fig. 9. HR and Rf short vs. long range DFA timescaling exponents.

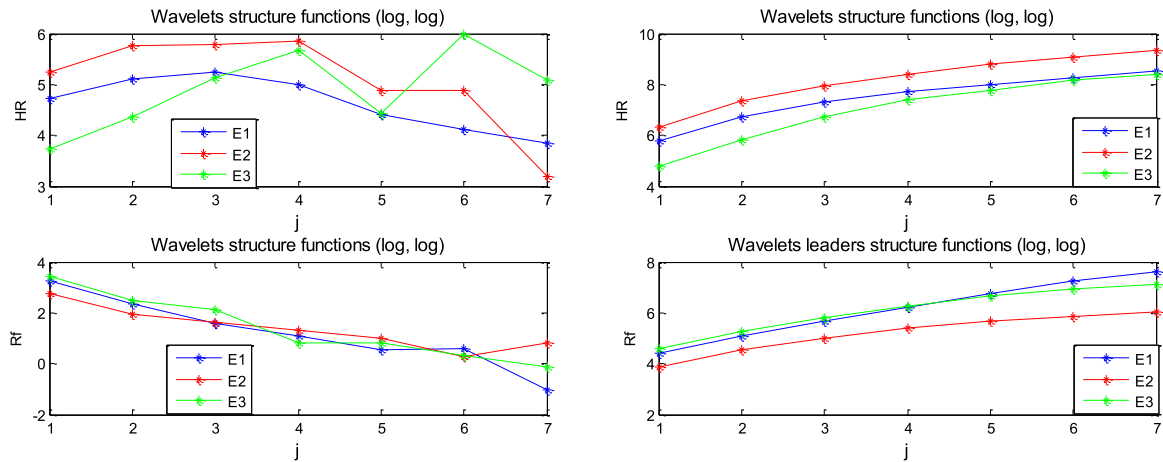


Fig. 10. Wavelet vs. wavelet leaders.

Table 8  
Short DFA  $\alpha_1^{HR}(j)/\alpha_1^{Rf}(j)$ .

$E_1$	$E_2$	$E_3$	$E_4$
1.33/0.64	1.62/0.65	1.49/0.74	1.43/0.65
1.31/0.72	1.32/0.63	1.49/0.67	1.41/0.70
1.34/0.71	1.34/0.64	1.44/0.67	1.48/0.69
1.27/0.74	1.38/0.64	1.44/0.55	
0.96/0.77	1.28/0.64	1.34/0.72	
1.30/0.75	1.44/0.73	1.42/0.69	
1.22/0.69	1.21/0.84	1.30/0.75	
1.19/0.76	1.20/0.76	1.24/0.72	
1.06/0.67	1.10/0.83	1.45/0.68	
1.19/0.68	1.32/0.71	1.38/0.67	

$\tau_1^{HR} > 1$  for 7 out of 10 Alpinists in  $E_1$ , 8 out of 10 Alpinists in  $E_2$  and 9 out of 10 Alpinists in  $E_3$ .

$\tau_1^{HR}(E_1) < \tau_1^{HR}(E_2)$  ( $\tau_1^{HR}$  increases at 3000 m) for 9 out of 10 Alpinists.

Table 10 (resp. Table 11) shows the short (resp. long) range wavelet leaders' exponents of HR vs. Rf over three or four steps and ten Alpinists (one row per Alpinist). Fig. 11 shows  $S_{HR}(j, 2)$  and  $S_{Rf}(j, 2)$  as a function of  $j$  for three steps and the corresponding short and long range scaling law exponents (6th line, Table 10).

The time series were not long enough to have a great number of scales and thus to obtain significant results.

**Table 9**

Long DFA  $\alpha_2^{HR}(j)/\alpha_2^{Rf}(j)$ .

$E_1$	$E_2$	$E_3$	$E_4$
0.93/0.78	0.87/0.70	0.96/0.82	0.79/0.91
0.86/0.86	0.82/0.90	0.91/0.70	0.98/0.72
0.96/0.80	0.82/0.71	0.88/0.77	0.85/0.80
0.86/0.80	0.75/0.81	0.88/0.71	
0.91/0.76	0.83/0.85	1.04/0.87	
0.78/0.75	1.01/1.13	0.75/0.74	
0.81/0.80	0.74/0.85	1.01/0.80	
0.72/0.80	0.73/0.79	0.71/0.72	
0.83/0.91	0.78/0.94	1.05/0.81	
0.79/0.59	0.77/0.57	1.18/0.70	

**Table 10**

Leaders exponents  $\tau_1^{HR}/\tau_1^{Rf}$ .

$E_1$	$E_2$	$E_3$	$E_4$
1.07/0.61	1.46/0.61	1.08/0.64	1.23/0.61
1.01/0.63	0.99/0.67	1.26/0.64	0.97/0.64
1.06/0.60	1.12/0.61	1.03/0.64	1.08/0.68
1.09/0.59	1.03/0.55	1.17/0.49	
0.70/0.60	1.14/0.55	1.13/0.55	
1.06/0.68	1.22/0.58	1.03/0.63	
1.01/0.68	1.01/0.70	1.12/0.62	
0.99/0.65	1.24/0.65	1.01/0.65	
0.77/0.64	0.81/0.57	0.97/0.62	
1.02/0.66	1.11/0.73	1.11/0.75	

**Table 11**

Leaders exponents  $\tau_2^{HR}/\tau_2^{Rf}$ .

$E_1$	$E_2$	$E_3$	$E_4$
0.53/0.35	0.63/0.31	0.43/0.40	0.39/0.39
0.41/0.35	0.37/0.38	0.47/0.39	0.36/0.32
0.34/0.32	0.45/0.36	0.38/0.35	0.37/0.39
1.09/0.59	1.03/0.55	1.17/0.49	
0.30/0.43	0.37/0.40	0.34/0.32	
0.34/0.50	0.49/0.52	0.31/0.36	
0.33/0.44	0.29/0.41	0.55/0.44	
0.26/0.42	0.31/0.41	0.28/0.37	
0.30/0.49	0.35/0.25	0.41/0.32	
0.34/0.30	0.32/0.34	0.58/0.45	

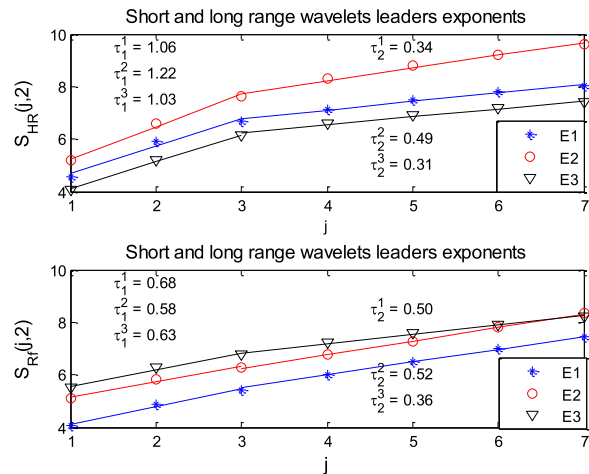


**Fig. 11.** HR and Rf wavelet leaders' exponents.

#### 4.4. Vertical speed

The vertical speed decreased by  $30\% \pm 8\%$  from 2500 to 4500 m of altitude ( $p = 0.003$ ). We observed that the ratio between HR and the vertical speed which gives the cardiac cost of the ascent (number of beats per meter) increased significantly ( $21 \pm 3$  vs.  $27 \pm 8$  cardiac beats per meter, at 2500 and 4500 m respectively,  $p < 0.01$ ). This was still more pronounced for the respiratory frequency over speed ratio (number of breaths per meter) ( $5 \pm 1$  vs.  $9 \pm 3$  breaths per meter, at 2500 and 4500 m respectively,  $p < 0.0001$ ).

### 5. Discussion

In accordance with our hypothesis, a high altitude mountain ascent modifies heart rate and respiratory frequency behaviors, but differently. This difference can be observed via physiological or mathematical analysis.

The aim of this paper was to study the effect of hypoxia on the HR and Rf variability, and the consequence of steep mountain trails in ice and snow conditions during the ascent of Mont Blanc (4808 m). It is a high summit of Europe's climbed by 20,000 climbers each year who are not aware of the physiological impact of such an effort in such conditions. Furthermore, we measured  $\text{SaO}_2$  but some walkers had cold hands and consequently blood circulation at the fingers did not allow for correct measurement [1]. In addition, we directly measured the oxygen uptake with gas exchange measurement [1]. That gave us  $\text{VO}_2$  which is the consequence of the cardiac output multiplied by the arterio-venous difference for oxygen ( $\text{Da-vO}_2$ ) in accordance with the Fick equation,  $\text{Da-vO}_2$  depending on  $\text{SaO}_2$ . That is why it is most important not to get  $\text{SaO}_2$  but  $\text{VO}_2$  directly, even if of course  $\text{SaO}_2$  is one of the  $\text{VO}_2$  factors that is crucial for discussing the  $\text{VO}_2$  decrease, but it was not the focus of the present study.

However, even if our purpose was to analyze the global effect of such an ascent on the heart and respiratory rate's variability, we must look at prior work where we had particularly focused on hypoxia effects. Indeed, HR and Rf variability showed a different adaptation to the high altitude. Autonomic responses are crucial for adaptation to hypoxia. Acute hypoxia triggers several autonomic mechanisms, mainly in the respiratory system (e.g., the hyperventilation started by the peripheral chemoreceptor reflex) and in the cardiovascular system (e.g., sympathetic activation with heart rate and cardiac output increase to improve pulmonary and tissue perfusion). Breathing is a potentially confounding factor in evaluating the relationship between respiratory modulation of muscle sympathetic nerve activity (RMSNA) and HRV, since both are modulated by the mechanics of breathing [3–6]. Pulmonary stretch reflexes are implicated in modulation of RMSNA within a breathing cycle. RMSNA decreases during inspiration and peaks during expiration, and this effect is augmented at larger lung volumes [18]. Changes of nonlinear HRV are associated with several cardiovascular stressors. The decreased nonlinear HRV has been related to physical stress, aging and a variety of pathologic conditions such as stable coronary artery disease [19]. On the other hand, increased nonlinear HRV was also associated with physiological situations such as high exercise intensity levels and complicated ischemic heart disease where it has been shown to be predictive for ventricular fibrillation and sudden cardiac death [19–24]. Most of the studies that assessed the relation between HRV and acute hypobaric hypoxia reported a reduced linear HRV pattern consistent with an increased sympathetic tone and decreased parasympathetic tone [25].

Nonlinear indicators of HRV have been sparsely studied in these situations. Altitude induced changes in cardiac rhythm could explain the significant rate of sudden cardiac death at high altitudes. It has been reported that 30% of all deaths during mountain sports at altitude are attributable to sudden cardiac death, more likely in those who have had prior myocardial infarction, coronary artery disease, or coronary risk factors [26]. In addition, it has been seen that the occurrence of ventricular extra systoles is proportional to the altitude during acute hypoxia exposure in a healthy elderly man [25].

However, one must take into account that the normal ascent route on Mont Blanc is not uniform in terms in steepness and technical difficulty. There are parts of easy, almost horizontal trail which require just constant-pace walking and parts that involve some rudimentary rock and ice climbing. Experienced mountain climbers can voluntarily change their breathing style depending on the route.

The Mont Blanc so called “Royal Route” is one of the most popular but difficult routes, especially just before the “Gouter” Hut (arriving at almost 4000 m for the night). We published the paper on that point of importance of experience level on physiological responses, in particular on the energy cost of the ascent [1].

On easy terrain, they usually maintain a uniform breathing rate highly correlated with their steps which are short and effortless. On difficult parts, they must make large steps which sometimes require a significant physical effort depending on the terrain. Under these circumstances they usually make a full-stop after a few steps and then regain their oxygen level by breathing at rest for a certain period of time. Thus it is not surprising that the breathing rate seems to be more random than the heart rate, which has a much higher inertia than the breathing rate, cannot be changed voluntarily and does not immediately correlate with the terrain and footstep pattern. This simple intuitive observation does not require any sophisticated mathematical analysis, but can be deduced from the raw time series displayed versus time in seconds simultaneously with vertical velocity measured in meters per second.

Here we wanted to quantify by a statistical analysis the impact of such a global ascent and effort performed in natural extreme conditions on heart and respiratory rates as we previously published during the marathon [2]. Indeed, we consider that the ecological approach of the exercise must be done if we want to really estimate the impact of such an effort on the body.

The “Mont Blanc Royal Route” is available on Google earth and may be freely consulted, including photos of the terrain corresponding to some marked changes in heart and respiratory rate behaviors. It might be also valuable to make measurements during periods of rest and sleep, when breathing is also non-voluntary.

In this paper, we studied the heart rate (HR) and respiratory frequency (Rf) of ten healthy Alpinists simultaneously collected during a Mont Blanc ascent, from 2500 to 4500 m of altitude, in ice and snow conditions. We showed different fractal scaling and time frequency behaviors of HR and Rf time series in a high mountain ascent. We performed the HR and Rf local cosine4 transform to analyze power law exponents, low vs. total energy, and spectrum entropy over segmentation boxes.

We found that both time series, HR and Rf, were differently affected by altitude. Indeed, the Rf time series average values increased significantly ( $p = 0.0003$ ), opposite to HR and the Rf ratio of low over whole local spectrum energy decreased ( $p = 0.04$ ) in contrast to HR. On the other hand, HR local cosine4 power law exponents, in absolute values, increased with altitude ( $p < 0.003$ ) and its DFA short range exponents increased after the 3000 m of altitude ( $p < 0.03$ ) while those of Rf did not change. Our time series were not long enough to obtain significant results for WL exponents or to be studied using the multifractal analysis [15–17].

Furthermore, this study showed that Rf had a more random behavior than HR in the sense that Rf local cosine4 spectrum had a higher entropy compared to HR ( $p < 0.01$ ). Moreover, the difference between the Rf and the HR entropy increased with altitude. Also, the difference between the HR and the Rf local cosine4 power law exponents, in absolute values, increased with altitude ( $p = 0.05$ ).

In addition, the DFA used in this paper has been initially introduced by Peng et al. [13,14] and then used by Taqqu et al. [27] for characterizing long-range dependence properties of DNA sequences. This method has been reported to be sensitive enough to demonstrate the fatigue effect on short time series [14,27]. The Jun Zhuang et al. paper [24] was one of the first having analyzed the alteration in scaling behavior of heartbeat time series for professional shooting athletes from rest to exercise.

To go further with this study, the DMA algorithm [28] can be used to estimate time dependent Hurst exponents  $H(t)$ .

The Shannon entropy defined using the probability distribution function  $P(\tau)$  over the elementary clusters cells [29] can be next investigated.

Furthermore, since HR and Rf time series are not equally modified with altitude, we can expect some changes in their cross-correlations. Our next challenge will be to use the DCCA analysis [30] together with the cross-correlations test [31] and the cross-correlation of two non stationary processes [32] to estimate how the cross-correlations change during high altitude ascent.

## 6. Conclusion

Respiratory frequency and heart rate are differently altered by high mountain ascent with hypoxia conditions. This study showed that breathing frequency was more random than heart rate dynamics and this was still more pronounced with altitude.

To our knowledge, the local cosine4 transform of Coifman, Malvar and Meyer was never used to study this kind of physiological signal. It appears to be an efficient time frequency analysis which can be used to compare simultaneously recorded time series.

## Acknowledgments

This work was supported by grants from DIGITEO and Région Ile-de-France.

## References

- [1] V.L. Billat, M. Dupré, J.R. Karp, J.P. Koralsztein, Mountaineering experience decreases the net oxygen cost of climbing Mont Blanc 4808 m, *Eur. J. Appl. Physiol.* 108 (2010) 1209–1216.
- [2] V. Billat, L. Hamard, Y. Meyer, E. Wesfreid, Detection of changes in the fractal scaling of heart rate and speed in a marathon race, *Physica A* 388 (2009) 3798–3808.
- [3] M.S. Badr, J.B. Skatrud, J.A. Dempsey, Determinants of poststimulus potentiation in humans during NREM sleep, *J. Appl. Physiol.* 73 (1992) 1958–1971.
- [4] J.W. Bellville, B.J. Whipp, Kaufman, R.D. Swanson GD, K.A. Aqleh, D.M. Wiberg, Central and peripheral chemoreflex loop gain in normal and carotid body-resected subjects, *J. Appl. Physiol.* 46 (1979) 843–853.
- [5] A.J. Berger, R.A. Mitchell, J.W. Severinghaus, Regulation of respiration (first to three parts), *N. Engl. J. Med.* 297 (1977) 92–201.
- [6] M. Ursino, E. Magosso, G. Avanzolini, An integrated model of the human ventilatory control system: the response to hypoxia, *Clin. Physiol.* 21 (2001) 465–477.
- [7] M. Kanai, F. Nishihara, T. Shiga, H. Shimada, S. Saito, Alterations in autonomic nervous control of heart rate among tourists at 2700 and 3700 m above sea level, *Wilderness, Environ. Med.* 12 (2001) 8–12.
- [8] S. Mallat, A wavelet tour of signal processing, in: *The Sparse Way*, Academic Press, Burlington MA, 2008.
- [9] H.S. Malvar, *Signal Processing with Lapped Transforms*, Artech House, Norwood, MA, 1992.
- [10] Y. Meyer, *Ondelettes et Algorithmes Concurrents*, in: *Actualités Scientifiques et Industrielles*, vol. 1435, Hermann, Paris, 1992.
- [11] V.M. Wickerhauser, *Adapted Wavelet Analysis from Theory to Software*, A. K. Peters, Boston MA, 1994.
- [12] J.E. McLaughlin, G.A. King, E.T. Howley Jr., D.R. Bassett, Ainsworth BE Validation of the COSMED K4b2 portable metabolic system, *Int. J. Sports. Med.* 22 (2001) 280–284.

- [13] C.K. Peng, S. Havlin, H.E. Stanley, A.L. Goldberger, Quantification of scaling exponents and crossover phenomena in non stationary heartbeat time series, *Chaos* 5 (1995) 82–87.
- [14] C.K. Peng, S. Buldyrev, S.V. Havlin, M. Simons, H.E. Stanley, A.L. Goldberger, Mosaic organization of DNA nucleotides, *Phys. Rev. E* 49 (1994) 1685–1689.
- [15] S. Jaffard, Wavelet techniques in multifractal analysis, in: M. Lapidus, M. van Frankenhuijsen (Eds.), *Fractal Geometry and Applications: Jubilee of Benoit Mandelbrot*, in: *Proceedings of Symposia in Pure Mathematics*, vol. 72 (2), AMS, 2004, pp. 91–152.
- [16] S. Jaffard, Multifractal formalism for functions, parts I and II, *J. Math. Anal.* 28 (1997) 944–998.
- [17] S. Jaffard, B. Lashermes, P. Abry, Wavelet leaders in multifractal analysis, in: T. Qian, M.I. Vai, X. Yuesheng (Eds.), *Applied and Numerical Harmonic Analysis*, Birkhäuser, Basel, Switzerland, 2007, pp. 201–246.
- [18] M.D. Brown, Metabolic control of blood flow with references to heart, skeletal muscle and brain, in: D. Jordan, J. Marshall (Eds.), *Cardiovascular Regulation*, Portland Press, London, UK, 1995, pp. 113–126.
- [19] A.L. Goldberger, C.K. Peng, L.A. Lipsitz, What is physiologic complexity and how does it change with aging and disease? *Neurobiol. Aging*. 23 (2002) 23–26.
- [20] P.C. Ivanov, L.A. Amaral, A.L. Goldberger, S. Havlin, M.G. Rosenblum, Z.R. Struzik, H.E. Stanley, Multifractality in human heartbeat dynamics, *Nature* 399 (1999) 461–465.
- [21] N. Iyengar, C.K. Peng, R. Morin, A.L. Goldberger, L.A. Lipsitz, Age-related alterations in the fractal scaling of cardiac interbeat interval dynamics, *Am. J. Physiol.* 271 (1996) R1078–R1084; *Physica A* 387 (2008) 6553–6557.
- [22] D.T. Kaplan, M.I. Furman, S.M. Pincus, S.M. Ryan, L.A. Lipsitz, A.L. Goldberger, Aging and the complexity of cardiovascular dynamics, *Biophys. J.* 59 (1991) 945–949.
- [23] R. Kitney, D. Linkens, A. Selman, A. McDonald, The interaction between heart rate and respiration: part II–nonlinear analysis based on computer modeling, *Automedica* 4 (1982) 141–153.
- [24] J.J. Zhuang, X. Ning, A.J. He, M. Zou, B. Sun, X.H. Wu, Alteration in scaling behavior of short-term heartbeat time series for professional shooting athletes from rest to exercise, *Physica A* 387 (2008) 6553–6557.
- [25] P.A. Easton, L.J. Slykerman, N.R. Anthonisen, Ventilatory response to sustained hypoxia in normal adults, *J. Appl. Physiol.* 61 (1986) 906–911.
- [26] T.G. Neilan, J.L. Januzzi, E. Lee-Lewandrowski, T.T. Ton-Nu, D.M. Yoerger, D.S. Jassal, K.B. Lewandrowski, A.J. Siegel, J.E. Marshall, P.S. Douglas, D. Lawlor, M.H. Picard, M.J. Wood, Myocardial injury and ventricular dysfunction related to training levels among nonelite participants in the Boston marathon, *Circulation* 114 (2006) 2325–2333.
- [27] M.S. Taqqu, M. Teverovsk, W. Willinger, Estimators for long range dependence: an empirical study, *Fractals* 3 (1995) 785–798.
- [28] A. Carbone, G. Castelli, H.E. Stanley, Time-dependent Hurst exponent in financial time series, *Physica A* 344 (2004) 267–271.
- [29] A. Carbone, H. Eugene Stanley, Scaling properties and entropy of long-range correlated time series, *Physica A* 384 (2007) 21–24.
- [30] Boris Podobnik, H. Eugene Stanley, Detrended cross-correlation analysis: a new method for analyzing two nonstationary time series, *Phys. Rev. Lett.* 100 (2008) 084102.
- [31] B. Podobnik, I. Grosse, D. Horvatić, S. Ilic, P.Ch. Ivanov, Stanley, Quantifying cross-correlations using local and global detrending approaches, *Eur. Phys. J. B* 71 (2009) 243–250.
- [32] Sergio Arianos, Anna Carbone, Cross-correlation of long-range correlated series, *J. Stat. Mech.* (2009) P03037.